

Design methods for steel fiber reinforced concrete industrial floors

J.A.O. Barros¹, A. Ventura Gouveia², J.M. Sena Cruz¹, J.A.B. Antunes³, A.F.M. Azevedo⁴
¹University of Minho, Portugal; ²Polytechnic Institute of Viseu, Portugal; ³Civitest Company, Portugal; ⁴University of Porto, Portugal

Abstract

Industrial floors are still the main application of steel fiber reinforced concrete (*SFRC*). Crack control joints are made to concentrate the crack propagation in these weakness-induced surfaces, resulting in a floor divided in panels. The design of a *SFRC* floor is currently made by means of the study of one of these panels, using the yield line method (*YLM*). The ultimate load of the panel depends on the maximum bending moment of the slab. Since in flooring applications the content of steel fibers, in general, does not exceed 45 kg/m³, the maximum bending moment is only slightly increased by the presence of steel fibers. Therefore, when the *YLM* is used to design this type of *SFRC* application the contribution of the fiber reinforcement cannot be accurately simulated. In the present work, this deficiency of the *YLM* is shown and justified by means of experimental and numerical research. Furthermore, the *YLM* is unable to predict the force-deflection relationship of a concrete slab supported on soil. The finite element method (*FEM*) is a powerful tool to analyze this type of structures. However, the accuracy of the analysis depends on the quality of the constitutive model used to simulate the nonlinear behavior of the intervening materials. For this purpose, an appropriate constitutive model was developed and is briefly described in the present work. This model is used in the analysis of *SFRC* slabs on soil. Using experimental results and applying the corresponding computational code, a numerical strategy for establishing design charts for *SFRC* slabs on soil is proposed.

Keywords: Material Nonlinear Analysis, Steel Fiber Reinforced Concrete, Smearred Crack Model, Finite Element Method, Yield Line Method.

Joaquim Barros, Assistant Prof.
Department of Civil Engineering
School of Engineering, University of Minho
4800-058 Campus de Azurém, Guimarães
Portugal

Email: barros@civil.uminho.pt
Tel.: +351 253 510 200

1.0 Introduction

A research project was carried out to characterize the properties and to develop a cost competitive steel fiber reinforced concrete (*SFRC*) applicable to floors of industrial buildings [1, 2]. In this project the influence of the percentage of cement replaced by fly ash, the concrete age, the fiber aspect-ratio and the content of fibers on the mechanical properties of the *SFRC* was analyzed. The compositions and the obtained main properties are published elsewhere [1]. The main objective of the experimental program was the characterization of the post-cracking behavior of this material. For this purpose, notched beams were subject to three point bending tests according to the recommendations of RILEM TC 162-TDF [3]. This research project is also devoted to the development of a design approach for industrial floors. In order to avoid the formation of uncontrolled cracks due to shrinkage and temperature variation, crack control joints are opened, dividing the floor into panels. The design of a *SFRC* floor is, in general, restricted to the analysis of a representative panel. The fiber suppliers, in general, recommend the use of the yield line method (*YLM*) to design this type of applications [4]. According to the *YLM* the load carrying capacity of a concrete slab depends on the maximum bending moment of the slab, M . Therefore, the contribution of the fiber reinforcement can only be simulated by the *YLM* when M increases with the content of fibers, Q_f . In order to verify this observation, the values of M were obtained in concrete specimens reinforced with 15, 25, 35 and 45 kg/m³ of Dramix[®] RC-65/60 hooked end steel fibers. In these experiments the compositions do not incorporate fly ash and the properties were obtained at the age of 28 days. The properties of these concretes can be found elsewhere [1, 2]. In the present work the values of M are calculated with a cross-section layered model (*CSLM*) that takes into account the constitutive laws of the intervening materials and the kinematic and equilibrium conditions [2]. In the *CSLM*, the *SFRC* post-cracking behavior is modeled by a stress-crack opening diagram, that is defined by performing inverse analysis in order to fit, with acceptable error, the force deflection relationships obtained in the three point bending notched beam tests carried out according to the RILEM TC 162-TDF. The *CSLM* provides the moment-curvature, $M-\chi$, and moment-crack opening, $M-w$, relationships of a cross section. The performance of the fiber reinforcement is not affected by environmental aggressions when the crack width does not exceed 0.3 mm and normal conditions are considered [5]. For this reason the value of M used to evaluate the load carrying capacity of the slab according to the *YLM* is the maximum moment up to a crack opening of 0.3 mm (M_R). The force values corresponding to this load carrying capacity are referred by F_{YLM} and are compared with the results obtained with the finite element method. In this case the force is termed F_{FEM} . In the *FEM* simulation a material nonlinear analysis was performed considering an elasto-plastic multi-fixed smeared crack model [6]. The influence of the slab thickness, h , the soil reaction modulus, K_s , and the content of fibers, Q_f , was analyzed by means of a parametric study where h was considered equal to 120, 160, 200 or 240 mm, K_s equal to 0.01, 0.04 or 0.08 N/mm³ and Q_f equal to 15, 25, 35 or 45 kg/m³. In all cases Dramix[®] RC-65/60 hooked ends steel fibers were used. Based on the values obtained with the *FEM* analysis, a chart is proposed for the design of *SFRC* slabs on soil.

2.0 Elasto-plastic multi-fixed smeared crack model for the *FEM* simulations

According to the present model, a concrete slab is considered a plane shell formulated under the Reissner-Mindlin theory [7]. In order to simulate the progressive damage induced by cracking and plasticity, the shell element is discretized in layers. Each layer is considered in a state of plane stress. The incremental strain vector derived from the incremental nodal displacements obtained under the framework of a nonlinear *FEM* analysis is decomposed in an incremental crack strain vector, $\Delta \underline{\epsilon}^{cr}$, and an incremental strain vector of the concrete between cracks, $\Delta \underline{\epsilon}^{co}$. This last

vector is decomposed in an elastic reversible part, $\Delta \underline{\underline{\varepsilon}}^e$, and an irreversible or plastic part, $\Delta \underline{\underline{\varepsilon}}^p$, resulting

$$\Delta \underline{\underline{\varepsilon}} = \Delta \underline{\underline{\varepsilon}}^{cr} + \Delta \underline{\underline{\varepsilon}}^{co} = \Delta \underline{\underline{\varepsilon}}^{cr} + \Delta \underline{\underline{\varepsilon}}^e + \Delta \underline{\underline{\varepsilon}}^p \quad (1)$$

2.1 – Concrete constitutive laws

The incremental stress vector can be computed from the incremental elastic strain vector,

$$\Delta \underline{\underline{\sigma}} = \underline{\underline{D}}^{co} \Delta \underline{\underline{\varepsilon}}^{co} \quad (2)$$

where $\underline{\underline{D}}^{co}$ is the concrete tangent constitutive matrix,

$$\underline{\underline{D}}^{co} = \begin{bmatrix} \underline{\underline{D}}_{mb}^{co} & \underline{\phi} \\ \underline{\phi} & \underline{\underline{D}}_s^{co} \end{bmatrix} \quad (3)$$

with $\underline{\underline{D}}_{mb}^{co}$ being the in-plane stiffness matrix and $\underline{\underline{D}}_s^{co}$ the out-of-plane shear stiffness matrix [8]. In the present model concrete behavior is assumed linear elastic in terms of out-of-plane shear. Therefore, the concrete nonlinear behavior is only considered in the $\underline{\underline{D}}_{mb}^{co}$ constitutive matrix.

2.1.1 - Linear elastic uncracked concrete

For linear elastic uncracked concrete, $\underline{\underline{D}}_{mb}^{co}$ is designated by $\underline{\underline{D}}_{mb}^{eco}$ being defined elsewhere [8].

2.1.2 - Linear elastic cracked concrete

In cracked concrete, with the concrete between cracks in linear elastic state, $\underline{\underline{D}}_{mb}^{co}$ is replaced in (3) with $\underline{\underline{D}}_{mb}^{ecrco}$. This matrix is defined with the following expression [6]

$$\underline{\underline{D}}_{mb}^{co} \Rightarrow \underline{\underline{D}}_{mb}^{ecrco} = \underline{\underline{D}}_{mb}^{eco} - \underline{\underline{D}}_{mb}^{eco} \left[\underline{\underline{T}}^{cr} \right]^T \left(\hat{\underline{\underline{D}}}^{cr} + \underline{\underline{T}}^{cr} \underline{\underline{D}}_{mb}^{eco} \left[\underline{\underline{T}}^{cr} \right]^T \right)^{-1} \underline{\underline{T}}^{cr} \underline{\underline{D}}_{mb}^{eco} \quad (4)$$

where $\underline{\underline{T}}^{cr}$ is a transformation matrix that depends on the direction of the cracks formed at a sampling point and $\hat{\underline{\underline{D}}}^{cr}$ is the constitutive matrix of the set of cracks. Each crack is governed by the following constitutive relationship

$$\Delta \underline{\underline{\sigma}}_t^{cr} = \underline{\underline{D}}^{cr} \Delta \underline{\underline{\varepsilon}}_t^{cr} \quad (5)$$

where $\Delta \underline{\underline{\sigma}}_t^{cr}$ is the incremental local crack stress vector. This vector has the following components,

$$\Delta \underline{\underline{\sigma}}_t^{cr} = \left[\Delta \sigma_n^{cr} \quad \Delta \tau_t^{cr} \right]^T \quad (6)$$

In this equation, $\Delta \underline{\underline{\varepsilon}}_t^{cr}$ is the incremental crack strain vector, which has the following components

$$\Delta \underline{\underline{\varepsilon}}_t^{cr} = \left[\Delta \varepsilon_n^{cr} \quad \Delta \gamma_t^{cr} \right]^T \quad (7)$$

and

$$\underline{\underline{D}}^{cr} = \begin{bmatrix} D_I^{cr} & 0 \\ 0 & D_{II}^{cr} \end{bmatrix} \quad (8)$$

is the crack stiffness matrix, where D_I^{cr} and D_{II}^{cr} are the fracture mode I and the fracture mode II stiffness modulus of the smeared cracks, respectively. In (8) D_I^{cr} is characterized by the fracture parameters, namely the stress at crack initiation, $\sigma_{n,1}^{cr}$ (see Fig. 1), the fracture energy, G_f , the shape of the softening law and the crack band width, l_b . In smeared crack models the fracture zone is distributed over l_b , which must depend on the finite element geometric characteristics in order to assure that the results of the *FEM* analysis are not dependent on the finite element mesh [9].

Therefore, $\Delta\varepsilon_n^{cr} = \Delta w/l_b$, where Δw is the total crack opening displacement increment in the crack band width. In the present numerical simulation l_b is assumed to be equal to the square root of the area associated with an integration point. Fiber reinforcement behavior is mainly influenced by the fracture energy and by the shape of the softening branch. Previous research has shown that the trilinear $\sigma_n^{cr} - \varepsilon_n^{cr}$ diagram represented in Fig. 1 is suitable for the simulation of the fracture mode I of the *SFRC* [2].

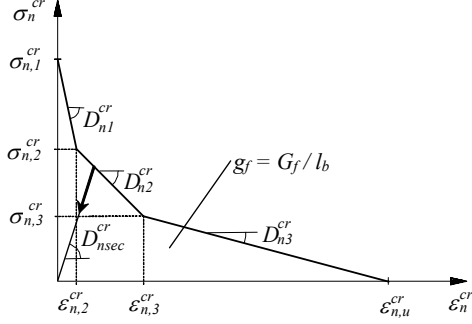


Figure 1. Tri-linear tensile-softening diagram.

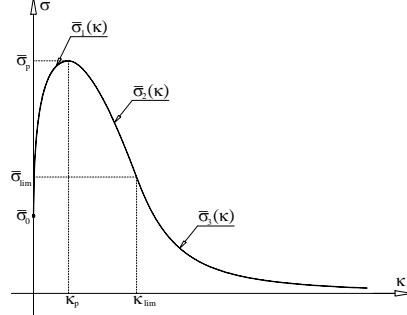


Figure 2. Hardening/softening diagram.

The fracture mode II modulus, D_{II}^{cr} , is obtained with the following expression [7]

$$D_{II}^{cr} = \frac{\beta}{1-\beta} G_c \quad (9)$$

where G_c is the concrete elastic shear modulus and β is the shear retention factor, which is defined by

$$\beta = \left(1 - \frac{\varepsilon_n^{cr}}{\varepsilon_{n,u}^{cr}} \right)^{p_1} \quad (10)$$

In this equation p_1 is an integer parameter that can assume distinct values in order to simulate different levels of concrete shear stiffness degradation [7].

2.1.3 - Elasto-plastic uncracked concrete

In the elasto-plastic uncracked concrete, the in-plane material stiffness matrix \underline{D}_{mb}^{co} of (3) is replaced with $\underline{D}_{mb}^{epco}$. This matrix is obtained with the following expression [6]

$$\underline{D}_{mb}^{co} \Rightarrow \underline{D}_{mb}^{epco} = \underline{H} - \frac{\underline{H} \frac{\partial f}{\partial \underline{\sigma}} \left(\frac{\partial f}{\partial \underline{\sigma}} \right)^T \underline{H}}{h + \left(\frac{\partial f}{\partial \underline{\sigma}} \right)^T \underline{H} \frac{\partial f}{\partial \underline{\sigma}}} \quad (11)$$

where,

$$\underline{H} = \left(\left[\underline{D}_{mb}^{eco} \right]^{-1} + h_c \Delta \lambda \frac{\partial^2 f}{\partial \underline{\sigma}^2} \right)^{-1} \quad (12)$$

$\partial f / \partial \underline{\sigma}$ is the flow vector and h_c is a scalar function that depends on the hydrostatic pressure [6]. The aim of h_c is the amplification of the contribution of $\Delta \lambda \partial f / \partial \underline{\sigma}$ to the plastic strain increment vector, $\Delta \underline{\varepsilon}^p$

$$\Delta \underline{\varepsilon}^p = \Delta \lambda h_c \frac{\partial f}{\partial \underline{\sigma}} \quad (13)$$

In (12) $\Delta \lambda$ is the variation of the plastic multiplier, which was assumed to be equal to the variation of the hardening parameter, $\Delta \kappa$, since a strain-hardening hypothesis was assumed. For the amount of fibers used in industrial floors, experimental research has shown [10, 11] that the shape of the yield surface, f , of *SFRC* under biaxial stress state is similar to the yield surface of the corresponding plain concrete. Therefore the yield surface proposed by Owen and Figueiras,

$$f(\underline{\sigma}, \kappa) = \left(\underline{\sigma}^T \underline{P} \underline{\sigma} \right)^{1/2} + \underline{q}^T \underline{\sigma} - \bar{\sigma}(\kappa) = 0 \quad (14)$$

was adopted in the present model, where \underline{P} is the projection matrix and \underline{q} is the projection vector [6]. Fig. 2 represents the relationship between the yield stress, $\bar{\sigma}$, and the hardening parameter, κ , used to simulate the hardening and softening phases of plain concrete behavior. This relationship was also used in *SFRC* applications, since for the amount of fibers used in flooring applications the concrete uniaxial compression behavior is not affected by the presence of fibers. The expressions of $\bar{\sigma}_i(\kappa)$ are published in [6].

2.1.4 - Elasto-plastic cracked concrete

For the case of cracked concrete with concrete between cracks exhibiting an elasto-plastic behavior, \underline{D}_{mb}^{co} of (3) is replaced with $\underline{D}_{mb}^{epcrco}$. This matrix is defined with the following expression [6]

$$\underline{D}_{mb}^{co} \Rightarrow \underline{D}_{mb}^{epcrco} = \underline{D}_{mb}^{epco} - \underline{D}_{mb}^{epco} \left[\underline{T}^{cr} \right]^T \left(\hat{D}^{cr} + \underline{T}^{cr} \underline{D}_{mb}^{epco} \left[\underline{T}^{cr} \right]^T \right)^{-1} \underline{T}^{cr} \underline{D}_{mb}^{epco} \quad (15)$$

where $\underline{D}_{mb}^{epco}$ was defined in (11).

2.2 – Soil

The soil is simulated with springs that are orthogonal to the laminate structure. The evaluation of the tangent soil reaction modulus can be performed with plate-loading tests [12]. The results of these tests have revealed that the soil pressure-settlement relationship may be simulated with a multilinear or linear-parabolic diagram [8, 12]. The soil contribution to the stiffness of the whole structural system is computed by adding the soil stiffness matrix,

$$\underline{K}_{so}^{(e)} = \int_{A^{(e)}} \underline{N}^T K_s \underline{N} dA \quad (16)$$

to the slab stiffness, where $A^{(e)}$ is the area of a finite element and \underline{N} is the vector of the element shape functions. In (16) K_s is the tangent soil reaction modulus. The friction between the slab and the soil is neglected. When the concrete slab loses contact with the soil in a sampling point, the part of the soil that corresponds to this sampling point does not contribute to the stiffness of the slab-soil system.

3.0 YLM versus FEM analysis

3.1 – SFRC fracture parameters and maximum bending moment of the slabs cross section

Applying an inverse analysis, as described in [13], in order to fit the force-deflection relationships obtained in the three point notched *SFRC* beam tests carried out according to RILEM TC 162-TDF recommendations, the parameters defining the $\sigma_n^{cr} - \varepsilon_n^{cr}$ diagram depicted in Fig. 1 were obtained.

These values are indicated in Table 1.

Table 1 – Parameters defining the diagram of Fig. 1 for the cost competitive SFRC

Q_f (kg/m ³)	$\sigma_{n,1}^{cr}$ (MPa)	$\frac{\sigma_{n,2}^{cr}}{\sigma_{n,1}^{cr}}$	$\frac{\sigma_{n,3}^{cr}}{\sigma_{n,1}^{cr}}$	$\frac{\varepsilon_{n,2}^{cr}}{\varepsilon_{nu}^{cr}}$	$\frac{\varepsilon_{n,3}^{cr}}{\varepsilon_{nu}^{cr}}$	w_2 (mm)	w_3 (mm)	w_4 (mm)	G_f (N/mm)
15	2.40	0.35	0.11	2.55	0.10	0.101	3.969	3.975	2.30
25	2.60	0.51	0.31	1.28	0.79	0.053	3.279	4.164	3.90
35	1.95	0.70	0.22	2.97	0.63	0.160	3.389	5.398	3.60
45	3.42	0.60	0.60	0.05	0.14	0.003	0.812	5.614	6.60

For the evaluation of the maximum bending moment, M , a *CSLM*, as described in [14], was used. In the *CSLM*, the concrete post-cracking behavior is simulated with a trilinear stress-crack opening σ - w diagram derived from the $\sigma_n^{cr} - \varepsilon_n^{cr}$ diagram represented in Fig. 1. In order to convert $\sigma_n^{cr} - \varepsilon_n^{cr}$ into $\sigma_n^{cr} - w$, the following relationship was assumed: $w = \varepsilon_n^{cr} l_b$. In the present work l_b was considered equal to the square root of the area of the integration points of the finite elements that were considered in material nonlinear regime (see Fig. 5), resulting $l_b = 100$ mm. According to this strategy, the values obtained for w_i are indicated in Table 1.

Applying the *CSLM* and the values indicated in Table 1, the maximum moment up to a crack opening of 0.3 mm (M_R) was obtained for slabs with distinct thickness and built with the cost competitive SFRC proposed in the research project. The obtained M_R values are included in Table 2. It can be verified that for $Q_f < 45$ kg/m³ the maximum moment has occurred for a crack opening, w_R , less than 0.3 mm. For $Q_f = 45$ kg/m³ the maximum moment up to $w = 0.3$ mm occurred at this crack opening value. The values included in Table 2 indicate that the fiber influence in terms of M_R is only significant for $Q_f = 45$ kg/m³.

Table 2 – Maximum moment up to a crack opening of 0.3 mm (M_R).

h [mm]	Q_f [kg/m ³]	M_R [kN.m/m]	w_R [mm]
120	15	10.55	0.034
	25	10.70	0.022
	35	10.11	0.092
	45	12.80	0.300
160	15	18.74	0.032
	25	19.07	0.024
	35	17.94	0.100
	45	22.78	0.300
200	15	29.25	0.031
	25	29.82	0.025
	35	28.11	0.072
	45	35.70	0.300
240	15	42.16	0.039
	25	42.97	0.026
	35	40.53	0.079
	45	51.56	0.300

3.2 – Design according to the YLM

The design of a SFRC floor is, in general, restricted to the analysis of a representative panel. The fiber suppliers are recommending the use of the *YLM* to design this type of structures. For the most common situations a point load in a corner of the panel is the most unfavorable load configuration, see Fig. 3. According to the *YLM*, when a load F , uniformly distributed in an area corresponding to a quarter of circle of radius $2a$, is applied in the corner of a panel, the ultimate load can be obtained from the following expression [4]

$$F = \frac{2M}{1 - \sqrt{a/L}/1.8} \left[1 + \frac{11\gamma(a/L)^2}{1 - \sqrt{a/L}/1.8} \right], \quad L = \sqrt[4]{\frac{E_c h^3}{12(1-\nu_c^2)}} / K_s, \quad \gamma = 0.259 - 0.0899\sqrt{a/L} \quad (17)$$

where M is the negative maximum bending moment of the slab, K_s is the soil reaction modulus, E_c

and ν_c are the concrete Young's Modulus and Poisson coefficient, and h is the slab thickness.

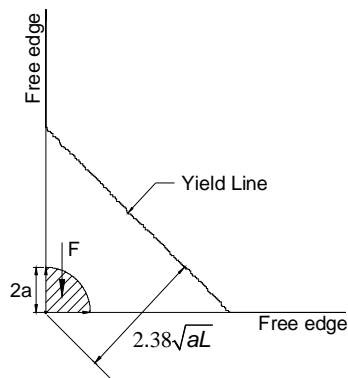


Figure 3. Yield line in a concrete panel loaded in a corner.

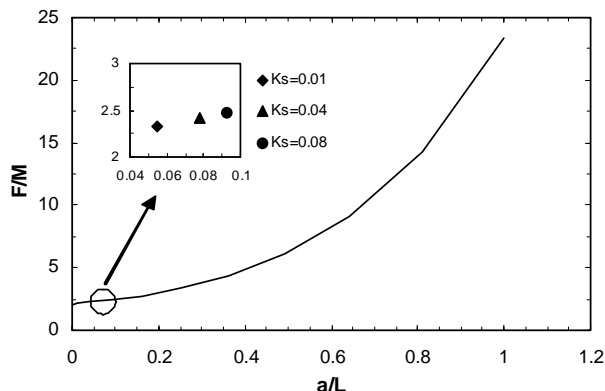


Figure 4. Relationship between F/M and a/L .

Replacing in (17) M with M_R values from Table 2, the ultimate load according to the YLM , designated by F_{YLM} , is obtained. These values are indicated in Table 3, showing that increasing the value of K_s and keeping constant the values of the remaining variables, the increase of the F_{YLM} is marginal. This can be justified by the quasi-constant value of the F/M ratio for the a/L values considered in the context of the present work (see (17) and Fig. 4). The ratio F/M only increases significantly for values of a/L above 0.2, which correspond to values of slab thickness, soil reaction modulus and loaded area not used in common flooring applications. Fig. 4 includes the example of a slab with $h=160$ mm and $Q_f=25$ kg/m³. For the K_s values considered, a/L is less than 0.1, resulting in a variation between 2.32 and 2.47 for the relationship between F/M and a/L . From the analysis of the values of F_{YLM} it is verified that for a given slab thickness, F_{YLM} did not change significantly up to a fiber content of 35 kg/m³. This is justified by the similar values of M_R for $Q_f \leq 35$ kg/m³ (see Table 2). Table 2 shows that for $Q_f \leq 35$ kg/m³ M_R has occurred at a very low crack opening values. For these w_R values the fiber reinforcing mechanisms are not yet activated. Therefore, for the amount of fibers used in flooring practice the YLM cannot take into account, directly, the benefits provided by the addition of fibers to concrete.

3.3 – Design according to the *FEM*

The performance of the elasto-plastic multi-fixed smeared crack model has already been appraised [7, 8]. This model was recently implemented in the release 4.0 of FEMIX computational code [6], and several enhancements were introduced in the original model in order to increase its numerical robustness. In the current section this model was applied to analyze the behavior of the 5×5 m² panel represented in Fig. 5, where the adopted finite element mesh is also shown. Since the elements outside the square of dashed line are not affected by any concrete nonlinear phenomena, they are assumed to behave linearly. The elements in the interior of this square were assumed to have a nonlinear material behavior. The panel thickness was decomposed in 10 layers of equal thickness. The *SFRC* fracture parameters indicated in Table 1 were used to define the $\sigma_n^{cr} - \varepsilon_n^{cr}$ trilinear diagram adopted to model the fracture mode I. Average compressive strength of 38 MPa and a Young's Modulus of 32 GPa were considered in the analysis. The compressive strength was evaluated in cubic specimens of 150 mm edge. Fig. 6 represents the crack pattern for the slab with $h=160$ mm, $Q_f=25$ kg/m³ and $K_s=0.01$ N/mm³, at a load level corresponding to a maximum crack width of 0.3 mm.

Table 3 – Load carrying capacity according to the *YLM* (using M_R values) and *FEM* analysis (load corresponding to a crack opening of 0.3 mm)

h (mm)	Q_f (kg/m ³)	M_R (kN.m/m)	F_{YLM} (kN)			$F_{FEM(w_{0.3})}$ (kN)			$F_{FEM(w_{0.3})}/F_{YLM}$		
			K_s (N/mm ³)			K_s (N/mm ³)			K_s (N/mm ³)		
			0.01	0.04	0.08	0.01	0.04	0.08	0.01	0.04	0.08
120	15	10.55	25.02	26.22	27.04	24.59	28.57	32.42	0.98	1.09	1.20
	25	10.7	25.38	26.59	27.43	29.15	32.85	37.11	1.15	1.24	1.35
	35	10.11	23.98	25.13	25.91	32.98	42.62	43.54	1.38	1.7	1.68
	45	12.80	30.36	31.81	32.81	41.01	48.17	53.86	1.35	1.51	1.64
160	15	18.74	43.48	45.16	46.27	40.17	47.12	49.22	0.92	1.04	1.06
	25	19.07	44.24	45.95	47.08	46.99	55.36	57.39	1.06	1.20	1.22
	35	17.94	41.62	43.23	44.29	52.16	64.57	77.48	1.25	1.49	1.75
	45	22.78	52.85	54.89	56.24	66.36	77.40	83.14	1.26	1.41	1.48
200	15	29.25	66.88	69.10	70.54	57.08	64.87	73.08	0.85	0.94	1.04
	25	29.82	68.19	70.45	71.91	69.16	77.33	86.48	1.01	1.10	1.20
	35	28.11	64.28	66.41	67.79	76.38	88.29	100.94	1.19	1.33	1.49
	45	35.70	81.63	84.34	86.09	97.87	113.55	121.63	1.20	1.35	1.41
240	15	42.16	95.40	98.21	100.00	77.87	90.88	94.80	0.82	0.93	0.95
	25	42.97	97.23	100.10	101.92	94.37	108.30	112.71	0.97	1.08	1.11
	35	40.53	91.71	94.41	96.14	105.25	118.61	128.53	1.15	1.26	1.34
	45	51.56	116.67	120.11	122.30	136.61	152.66	167.28	1.17	1.27	1.37

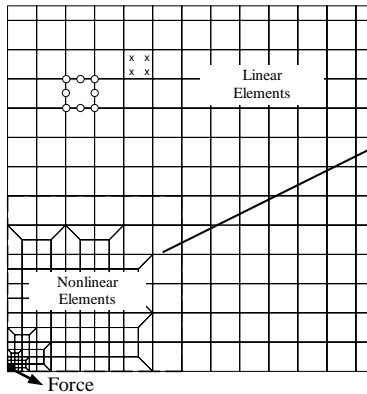


Figure 5. Finite element mesh.

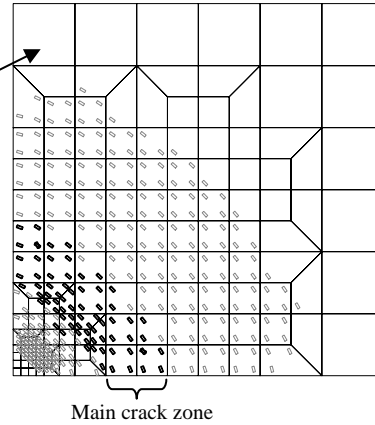


Figure 6. Crack pattern in the slab top surface at a load level corresponding to $w_{0.3}$ ($h=160\text{mm}$, $Q_f=25\text{ kg/m}^3$ and $K_s=0.01\text{ N/mm}^3$).

Figure 7 depicts a typical force-corner deflection relationship up to the moment when a maximum crack opening of 0.3 mm ($w_{0.3}$) occurred. In this figure one can observe the loads for a maximum crack width corresponding to the w_R indicated in Table 2 (designated by $F_{FEM(w_R)}$) and the loads for $w_{0.3}$ ($F_{FEM(w_{0.3})}$). The values of $F_{FEM(w_{0.3})}$ are indicated in Table 3. Since for $Q_f \leq 35\text{ kg/m}^3$ w_R are

too small to mobilize the fiber reinforcing mechanisms (see Table 2), the $F_{FEM(w_R)}$ values of the slabs reinforced with $Q_f \leq 35 \text{ kg/m}^3$ are similar. For the $F_{FEM(w_{0.3})}$ values, the effects of the fibers are visible, i.e., the load carrying capacity increases with the content of fibers, even for $Q_f \leq 35 \text{ kg/m}^3$, which was not the case when applying the *YLM*.

4.0 Strategy to built charts for the design of *SFRC* slabs on soil

The force values, $F_{FEM(w_{0.3})}$, obtained by *FEM* analysis, and the values of the corresponding variables of the parametric study (h , K_s and Q_f) are organized in order to define a chart from which the most economic solution for a *SFRC* slab supported on soil can be determined. This chart is represented in Fig. 8 and its applicability is only restricted to the conceived and characterized *SFRC* and for the load configuration considered in the present work (corner load). For instance, when a load of 90 kN is acting on the corner of a slab supported on a soil with $K_s=0.04 \text{ N/mm}^3$, the following solutions are obtained (see Fig. 8): $Q_f=15 \text{ kg/m}^3$ and $h=238 \text{ mm}$; $Q_f=25 \text{ kg/m}^3$ and $h=216 \text{ mm}$; $Q_f=35 \text{ kg/m}^3$ and $h=202 \text{ mm}$; $Q_f=45 \text{ kg/m}^3$ and $h=174 \text{ mm}$. Taking into account the prices of the concrete and fibers, the most economic solution can be selected.

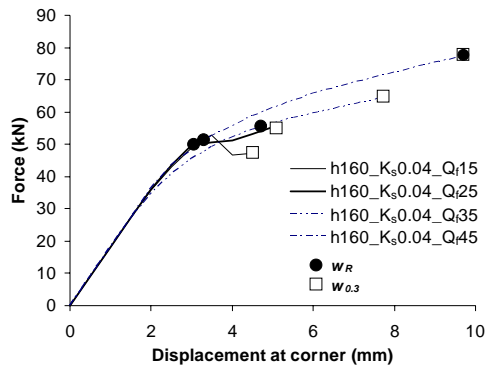


Figure 7. Relationship between the force and the deflection at the slab corner up to w_R and $w_{0.3}$.

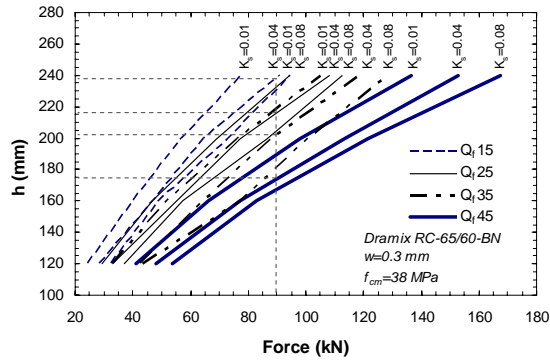


Figure 8. Design chart.

5.0 Conclusions

In the present work the applicability of the yield line method (*YLM*) for the analysis of industrial floors built with steel fiber reinforced concrete (*SFRC*) is assessed using the results obtained in a experimental research program where a cost competitive *SFRC* was conceived and their properties characterized. For this purpose, the results obtained with the *YLM* were compared with those calculated with a computer program based on the finite element method (*FEM*) in which an elasto-plastic smeared crack model was implemented. In this comparison, the influence of the slab thickness (h), the soil reaction modulus (K_s) and the amount of fibers (Q_f) was taken into account. The ultimate force obtained with the *YLM* depends on the maximum bending moment (M_R) of the *SFRC* slab. To evaluate M_R , a cross section layered model was used. Since in industrial floors Q_f , in general, does not exceed 45 kg/m^3 , M_R values are similar for *SFRC* slabs with $Q_f \leq 35 \text{ kg/m}^3$. Considering that F_{YLM} and $F_{FEM(w_{0.3})}$ designate the load carrying capacity of a *SFRC* floor determined with *YLM* and *FEM*, Table 3 shows that $F_{FEM(w_{0.3})}/F_{YLM}$ increased with Q_f and K_s . In

general, $F_{FEM(w_{0.3})}/F_{YLM} > 1$ for *SFRC* slabs with $Q_f > 15 \text{ kg/m}^3$ and supported on a soil with $K_s > 0.01 \text{ N/mm}^3$, showing that *YLM* is not capable of taking into account, directly, the benefits provided by fiber reinforcement in real flooring conditions. For *SFRC* slabs with $Q_f = 15 \text{ kg/m}^3$, $F_{FEM(w_{0.3})}/F_{YLM} < 1$, mainly when supported on weak soils, which means that the *YLM* is not a safe design approach for these cases. The $F_{FEM(w_{0.3})}/F_{YLM}$ ratio decreased with the thickness of the floor, being less than unit in slabs with $h = 240 \text{ mm}$, supported on a soil with $K_s = 0.01 \text{ N/mm}^3$, and reinforced with $Q_f = 25 \text{ kg/m}^3$, which is a current fiber content in flooring applications. The particular values obtained in this research are restricted to the designed *SFRC* situations, but it is expected that the observed tendencies and the main conclusions can be extended to any *FRC*.

6.0 References

1. Barros, J.A.O.; Antunes, J.A.B., "Experimental characterization of the flexural behaviour of steel fibre reinforced concrete according to RILEM TC 162-TDF recommendations", RILEM TC 162 TDF Workshop, pp. 77-89, 20-21 March 2003.
2. Barros, J.A.O.; Cunha, V.M.C.F.; Ribeiro, A.F.; Antunes, J.A.B., "Post-cracking behaviour of steel fibre reinforced concrete", RILEM Materials and Structures Journal, in press, 2004.
3. Vanderwalle, L. et al., "Test and design methods for steel fibre reinforced concrete - Final Recommendation", Materials and Structures Journal, Vol.35, pp. 579-582, November 2002.
4. Baumann, R.A. and Weisgerber, F.E., Yield line analysis of slabs-on-grade. *Jour. Struct. Engrg.* ASCE, 1983, 109(7), 1553-1568.
5. Mangat, P.S.; Molloy, B.T.; Gurusamy, K. (1989), "Marine durability of steel fiber reinforced concrete of high water-cement ratio", Fiber Reinforced Cements and Concretes-Recent.
6. Sena-Cruz, J.M.; Barros, J.A.O.; Azevedo, A.F.M., "Elasto-plastic multi-fixed smeared crack model for concrete", Technical report 04-DEC/E-05, Dep. Civil Eng., University of Minho, 70 pp, June 2004.
7. Barros, J.A.O., "Comportamento do betão reforçado com fibras - análise experimental e simulação numérica (Behavior of *FRC* - experimental analysis and numerical simulation)", PhD Thesis, Civil Eng. Dept., Faculty of Engineering, University of Porto, Portugal, 1995 (in Portuguese).
8. Barros, J.A.O.; Figueiras, J.A., "Nonlinear analysis of steel fibre reinforced concrete slabs on grade", Computers & Structures Journal, Vol.79, No.1, pp. 97-106, January 2001.
9. Bazant, Z.P. and Oh, B.H., Crack band theory for fracture of concrete. Materials and Structures, RILEM, 1983, 16(93), 155-177.
10. Yin, W.S.; Su, E.C.M.; Mansur, M.A. and Hsu, T.T.C., Biaxial Tests of plain and fiber concrete. *ACI Materials Journal*, 1989, **86**(3), 236-243.
11. Traina, L.A. and Mansour, S.A., Biaxial strength and deformational behaviour of plain and steel fiber concrete. *ACI Materials Journal*, 1991, **88**(3), 354-362.
12. Barros, J.A.O.; Figueiras, J.A., "Experimental behaviour of fiber concrete slabs on soil", Journal Mechanics of Cohesive-frictional Materials, Vol. 3, pp. 277-290, 1998.
13. Cunha, V.M.C.F., "Análise experimental e numérica do comportamento à tracção de betão reforçado com fibras (Experimental and numerical analysis of *SFRC*)", Tese de Mestrado, Dep. Eng^a Civil da UM, Setembro de 2004.
14. Ribeiro, A.F., "Modelos de fenda discreta na simulação do comportamento em flexão de betão reforçado com fibras de aço (Discrete crack model for the simulation of the flexural behavior of *SFRC*)", MSc Thesis, Dep. Civil Eng. University of Minho, September 2004.